Validation of the Contour Method Considering the In-plane Displacements at the Cut Surface†

GADALLAH Ramy *, MURAKAWA Hidekazu **

Abstract

Welding residual stresses are one of the main factors influencing the engineering properties of welded structures, and should be taken into account during designing and manufacturing different products such as ships, bridges, etc. The contour method is one of the new powerful stress measurement techniques that is used for measuring residual stresses. In this method a welded component is cut normal to the weld line. Displacements normal to the cut surface are measured. Using the finite element method (FEM), residual stresses before the cut are then reconstructed from the measured displacements. However after cutting the part of interest, only displacements normal to the cut surface can be measured while in-plane displacements cannot be measured. Therefore, the main objective of this paper is to examine the influence of in-plane displacements on the quality of reproduced residual stresses using numerical simulation. In this paper, a computational approach is developed to numerically simulate the contour method. Welding residual stresses are evaluated when conventional and low transformation temperature (LTT) weld wires are used. Phase transformation is considered for LTT welds. The developed computational approach is then used to simulate the contour method and reconstruct the residual stresses using 1) both normal and in-plane displacements, and 2) using only normal displacements. Simulation results show a very good agreement between welding residual stresses as originally computed and the reproduced stresses when in-plane displacements are considered. Additionally, application of only the displacement normal to the cut surface; reproduces stresses with a good agreement with welding residual stresses and those reproduced considering in-plane displacements.

KEY WORDS: (Contour method), (Residual stresses), (In-plane displacements), (Finite element method), (Phase transformation), (Martensitic transformation start temperature), (LTT welding wires)

1. Introduction

Safety of welded high strength steel structures calls for precise knowledge of welding residual stresses which profoundly influence crack resistance and service load. In particular, tensile residual stresses generated in weld lines are of major concern for structural integrity assessment in industrial components. In-service tensile loads superimpose over weld residual stresses and in case these are tensile this results in a reduction of the maximum bearable load of the component. Further tensile residual stresses impair the fatigue and stress corrosion behavior of the component [1, 2]. Therefore, how to control and reduce welding tensile residual stresses is a vital task both in structural design and in welding processes.

Several mechanical as well as thermal in situ and post-weld treatment methods and combinations of these methods are available for application during or after welding in order to reduce detrimental tensile residual stresses or to generate beneficial compressive residual stresses. Preferable solutions should be concentrated on the production process and that is to say that it would be favorable to enable the generation of beneficial compressive residual stresses directly during the welding process [2]. Many researchers have reported significant reductions in tensile welding residual stresses and improvement in fatigue strength by using a low transformation temperature (LTT) filler material as compared to the joints welded with conventional filler

† Received on December 10, 2014
* Graduate Student
** Professor
Transactions of JWRI is published by Joining and Welding Research Institute, Osaka University, Ibaraki, Osaka 567-0047, Japan

wires [3 −6].

Darcis et al. [7] mentioned that, in these LTT alloys, martensitic transformation in an unconstrained specimen starts at around 200 ºC and ends right at ambient temperature. By contrast, normal steel welding alloys have transformation temperatures around 400 ºC – 600 ºC. Additionally, Thomas and Liu [8] reported that martensite has a lower density than austenite; in which there is a 4–5% increase in martensite volume with the austenite to martensite transformation. Because of that, phase transformation causes compressive residual stresses in LTT alloys at ambient temperature [7].

During the past years many different methods for measuring residual stresses in different types of components have been developed. Rossini et al. [9] reported that techniques to measure residual stresses may be classified as either destructive, semi destructive or non-destructive. The destructive and semi destructive techniques, called also mechanical method, are dependent on inferring the original stress from the displacement incurred by completely or partially relieving the stress by removing material. These methods rely on the measurement of deformations due to the release of residual stresses upon removal of material from the specimen. Sectioning, contour, hole-drilling, ring-core and deep-hole are the principal destructive and semi destructive techniques used to measure residual stresses in structural members. Non-destructive methods include x-ray, neutron diffraction, ultrasonic and magnetic methods. These techniques usually measure some parameter that is related to the stress.

Currently, the contour method has become one of the most powerful techniques that provides measurement of residual stresses normal to a plane of interest. This technique is based on elastic stress relaxation after part cutting (Bueckner's elastic superposition principle [10 – 12]). The ability to obtain a full 2D cross-sectional map of residual stresses with a single measurement process makes the contour method unique. The methodology of the contour method consists of four major steps: part cutting, contour displacements measurement, data processing and elastic calculations for obtaining stresses from the measured displacements [13 – 17].

To the best of the author's knowledge, there is no investigation available in the literature on the numerical implementation of the contour method for predicting welding residual stresses. A greater and deeper understanding of the contour method steps such as cutting and reproducing stresses, will give a good perception for the contour method. In the present work, a computational approach (using an in-house FEM program) has been developed for numerically applying the contour method. In addition, welding residual stresses are predicted using conventional and LTT weld wires while considering phase transformation for LTT welds. In that approach, both volume change and mechanical properties variation are considered for LTT weld wires. In the contour method, a welded component is cut and the normal displacements to the cut surface are measured. Using the FEM, the measured displacements are then applied to reproduce the residual stresses as before cutting. As it is well known, in the contour method; displacements normal to the cut surface are measurable, however in-plane displacements cannot be measured. Accordingly, it is significant to examine the influence of in-plane displacements on the quality of reproduced stresses using the simulated contour method.

2. The concept of the contour method

After welded component is cooled, the residual stresses due to welding are produced. The contour method starts with cutting the welded component at any plane of interest. Due to cutting, the cut surfaces are deformed due to the relaxation of residual stresses. This deformation is assumed to be elastic deformation. Displacements normal to the cut surfaces are measured and then processed. Using the FEM, the residual stresses before the cut are then reconstructed from the processed measured displacements.

In order to examine the influence of in-plane displacements on the quality of reproduced stresses, the contour method should be simulated. Accordingly to numerically validate the contour method, three main steps are performed namely welding, cutting, and reproducing stresses, as shown in **Fig. 1**. In the simulated welding step, produced residual stresses due to welding are computed. After welding is simulated, welded component is cut normal to the weld line. In order to numerically implement cutting, it mainly relies on the stiffness of elements. Cutting elements behave as other elements of the model during welding and cooling processes. In other words, cutting elements have the same properties as other elements in both welding and cooling steps. After cooling process is completed, the stiffness of certain elements (i.e. elements that represent cutting) becomes very small as compared to other element's stiffness; that means cutting is performed numerically. Created cut surfaces locally deform owing to the relaxation of residual stresses present before the cutting. However because the resulting displacements are quite small for engineering materials, deformed shape of the body is not modeled after the cutting step. On the other hand, in the reproducing stresses step since the calculations represent a linear elastic problem; the residual stresses before cutting are reproduced by applying the calculated displacements after cutting as forced-displacement boundary conditions to a stress-free model with an inverse sign to the mesh nodes at the cut surface.

Theoretically (**Fig. 1**), residual stresses due to welding σ_W and change of stresses due to the relaxation of residual stresses σ (u, v, w) must be equal in the magnitude, as shown in **Eq. (1)**. However in the FEM, since stresses are calculated in elements not at nodes; so there is an error of the FEM data processing resulted in the calculated stresses as shown in **Eq. (2)**. However, this error of FEM data processing can be minimized by reducing the element size that faces to the cut surface.

Theory: $\sigma_W + \sigma(u, v, w) = 0$ **(1)**

FEM: $\sigma_W + \sigma(u, v, w) \simeq 0$ **(2)**

where u is the displacement normal to cut surface and v and w are the in-plane displacements at the cut surface.

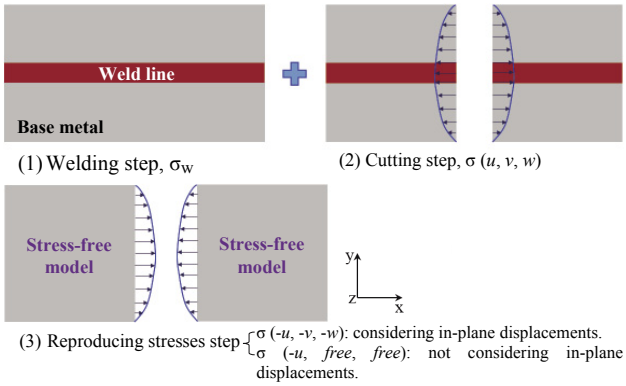

Fig. 1 Steps of the simulated contour method.

As mentioned above, practically, in-plane displacements at the cut surfaces cannot be measured. Therefore to examine the influence of in-plane displacements on the quality of reproduced residual stresses, the contour method can be numerically validated in two ways 1) by considering both normal and in-plane displacements $\sigma(-u, -v, -w)$ and 2) by considering only normal displacements $\sigma(-u, free, free)$; as shown in **Eqs. (3)** and **(4)**, respectively. Based on **Eqs. 1–4**, four cases are summarized in **Table 1**. In Case 1, both σ_W and σ_R are conformed theoretically. In Case 2, σ_W and σ_R are almost equal due to the error of FEM data processing. In Case 3, σ_W and σ_R are almost equal theoretically because the in-plane displacements are not taken into account. The absence of the in-plane displacements besides the error of FEM data processing make σ_W and σ_R are approximately equal, as in Case 4.

$$-\sigma(u, v, w) = \sigma(-u, -v, -w) = \sigma_R \quad \textbf{(3)}$$

$$-\sigma(u, v, w) \simeq \sigma(-u, free, free) = \sigma_R \quad \textbf{(4)}$$

where $\sigma(-u, -v, -w)$ is the calculated residual stress due to forcing both normal and in-plane displacements to the cut surface with the same values as after cutting but with inverse sign $(-u, -v, -w)$, σ_R is defined as reproduced residual stress, and $\sigma(-u, free, free)$ is the calculated residual stress due to forcing only the displacement normal to the cut surface $(-u)$ with keeping the in-plane displacements free to move (i.e. in-plane displacements are not forced to their original locations at the cut surface).

Table 1 Influence of in-plane displacements on reproduced stresses.

Case	Status	In-plane displacements	Assessment
1	Theory	Yes	$\sigma_W = \sigma_R$
2	FEM	Yes	$\sigma_W \simeq \sigma_R$
3	Theory	No	$\sigma_W \simeq \sigma_R$
4	FEM	No	$\sigma_W \approx \sigma_R$

3. Influence of element size at the cut surface

In order to verify the quality of the simulated contour method, element size faces to the cut surface should be properly selected. In addition, mesh density close to the cut surface should be carefully identified. Accordingly, a numerical study was carried out using three finite element (FE) models with the same size as 200 mm length, 160 mm width and 5 mm thickness. These FE models include different element sizes that face to the cut surface, besides different mesh densities around the cut surface as shown in **Fig. 2**. On the other hand, cutting was conducted at the mid-length of the three FE models normal to the weld line. In case of coarse and intermediate element sizes as in **Fig. 2 (a)** and **(b)**, respectively; the cutting zone mesh density (CZMD) is uniformly distributed around the cutting plane, at the mid-length of model, with the same size of these elements. However in case of the fine element size **(Fig. 2 (c))**, CZMD is gradually distributed from fine to coarse element from the cutting plane up to cutting zone edges. The cutting zone width is same for the three FE models as 20 mm wide. A bead-on-plate weld using gas metal arc welding (GMAW) process in the center and along the model length (i.e. from start to end of the model length) was performed with the same welding conditions for the three FE models. In this investigation, LTT wire was used for the three models. The welding conditions that used in the computational analyses were assumed as follows: welding current = 170 A, arc voltage = 15 V, welding speed = 300 mm/min, and arc efficiency = 80%.

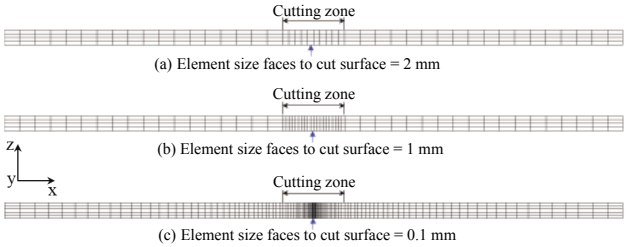

Fig. 2 Finite element models for examining the influence of element size that faces the cut surface. (a) coarse element size, (b) intermediate element size, and (c) fine element size.

Figure 3 shows that as the element size that faces to the cut surface becomes fine, the resulting longitudinal stresses after cutting become small. That's due to when the element size (i.e. mesh density) is fine enough, produced stresses are formed smoothly and gradually. However in case of a coarse element size that faces to the cut surface, the resulting stresses at the cut surface are high in magnitude and reveal sharp change in stresses due to the coarse mesh. Therefore in case of the fine element size, a very small longitudinal stress was produced after cutting. As mentioned above, in FEM there is an error in computed stresses due to FEM data processing; however, this error can be minimized by reducing the size of element that faces to the cut surface in which this is achieved as shown in **Fig.3**. Based on the reduction of the

resulting error due to FEM data processing, reproduced stresses σ_R can reveal a very good agreement with the originally induced stresses due to welding σ_W if the element size that faces to the cut surface is fine enough. Accordingly based on the results in **Fig. 3**, the fine element size (0.1 mm) and its CZMD were selected to be applied to the analysis model in the present study.

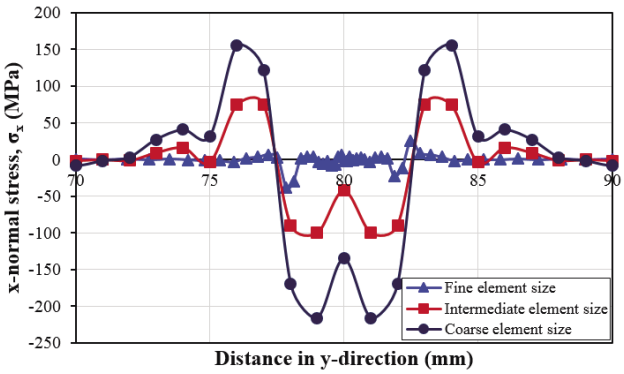

Fig. 3 Influence of the element size that faces the cut surface on the resulting longitudinal stresses. [Note: actual width of model is 160 mm].

4. Computational approach

Three main factors, namely volume change, yield strength variation and transformation induced plasticity (TRIP), have influences on the formation of welding residual stress in certain steels [18]. Practically, it is difficult to perform pure experiments in order to reveal the influence of each factor on the formation of welding residual stress because all factors occur almost at the same time during welding. However, it is possible to use numerical methods to clarify the influence of each factor on the welding residual stresses if the numerical method can quantitatively consider these factors [18]. However in the present study, TRIP factor is not considered.

In this study, an in-house thermal–elastic–plastic FEM program (JWRIAN) is developed in which the iterative substructure method is employed. This approach aims to reduce the computation time by dividing the model into regions which are linear or weakly non-linear and those which are highly non-linear. An iterative approach is used to ensure continuity of tractions between the linear and non-linear regions. Additionally, an algorithm which considers solid-state phase transformation is developed and employed. In this algorithm, phase transformation strain is computed and added to thermal strain. The thermal–elastic–plastic behavior is simulated using a sequentially coupled formulation in which thermal analysis is firstly completed to solve for thermal profiles. A mechanical analysis is subsequently executed which reads in the temperature profiles and solves for displacements, strains and stresses.

In this approach, the conventional Von Mises' elastic-plastic flow theory is considered. The total strain ε^{total} during the heating and cooling cycles of the welding process can be divided into the strain components given by **Eq. (5)**, namely, elastic strain ε^e, plastic strain ε^p, thermal strain ε^{th}, strain produced through phase transformation ε^{tr}, and creep strain ε^c, respectively. Then, the total strain increment can be expressed as shown in **Eq. (6)**.

$$\varepsilon^{total} = \varepsilon^e + \varepsilon^p + \varepsilon^{th} + \varepsilon^{tr} + \varepsilon^c \quad (5)$$

$$\Delta\varepsilon^{total} = \Delta\varepsilon^e + \Delta\varepsilon^p + \Delta\varepsilon^{th} + \Delta\varepsilon^{tr} + \Delta\varepsilon^c \quad (6)$$

where the thermal strain increment is expressed by following equation:

$$\Delta\varepsilon^{th} = \alpha(T)\,\Delta T \quad (7)$$

where α is the (temperature dependent) coefficient of thermal expansion and ΔT is the difference between a reference temperature and the material temperature. The strain increment contribution due to phase transformation $\Delta\varepsilon^{th}$ results from the volumetric change when the material exhibits a solid-state phase transformation. Shear strains internal to the material due to variant selection are not considered in this analysis.

4.1 Temperature-dependent materials data

In this study, conventional and LTT weld wires are employed. Both weld and base metals in case of conventional welded specimen are assumed to have the same mechanical properties. However in case of LTT welded specimens, two different mechanical properties are assumed for both weld and base metals. Temperature-dependent mechanical properties for phase A (austenite for weld and base metals), phase B (ferrite of both conventional weld metal and base metals) and phase C (martensite of LTT weld metals) are shown in **Fig. 4**. For both conventional and LTT welded specimens, when heating up to the austenitic start temperature (T_{As}) the temperature-dependent mechanical properties of phases B and C are considered; as shown in **Fig. 4 (b)** and **(c)**, respectively. After reaching the austenitic finish temperature (T_{Af}), and when by cooling until the ferritic/martensitic start temperature ($T_{Fs/Ms}$) is reached, the temperature-dependent mechanical properties of phase A; as shown in **Fig. 4 (a)**, are appropriate. Transformation is completed at the ferritic/martensitic finish temperature ($T_{Ff/Mf}$). In the region of phase transformation from ferrite/martensite to austenite ($T_{As} \rightarrow T_{Af}$) and again from austenite to ferrite/martensite ($T_{Fs/Ms} \rightarrow T_{Ff/Mf}$) a mixture law is applied. The thermal expansion coefficient of phase A is 2.2×10^{-5} 1/°C and for phases B and C is taken to be 1.5×10^{-5} 1/°C. In addition, temperature-dependent thermal physical properties of butt welded joint models are shown in **Fig. 5**.

4.2 Variation of yield strength due to microstructure change

As mentioned above, a mixture law is used in the current computational approach. Therefore, variations of mechanical properties (yield strength, Young's modulus and thermal expansion coefficient) due to microstructure change are considered. In this study, yield strength is taken as an example to explain how the mechanical

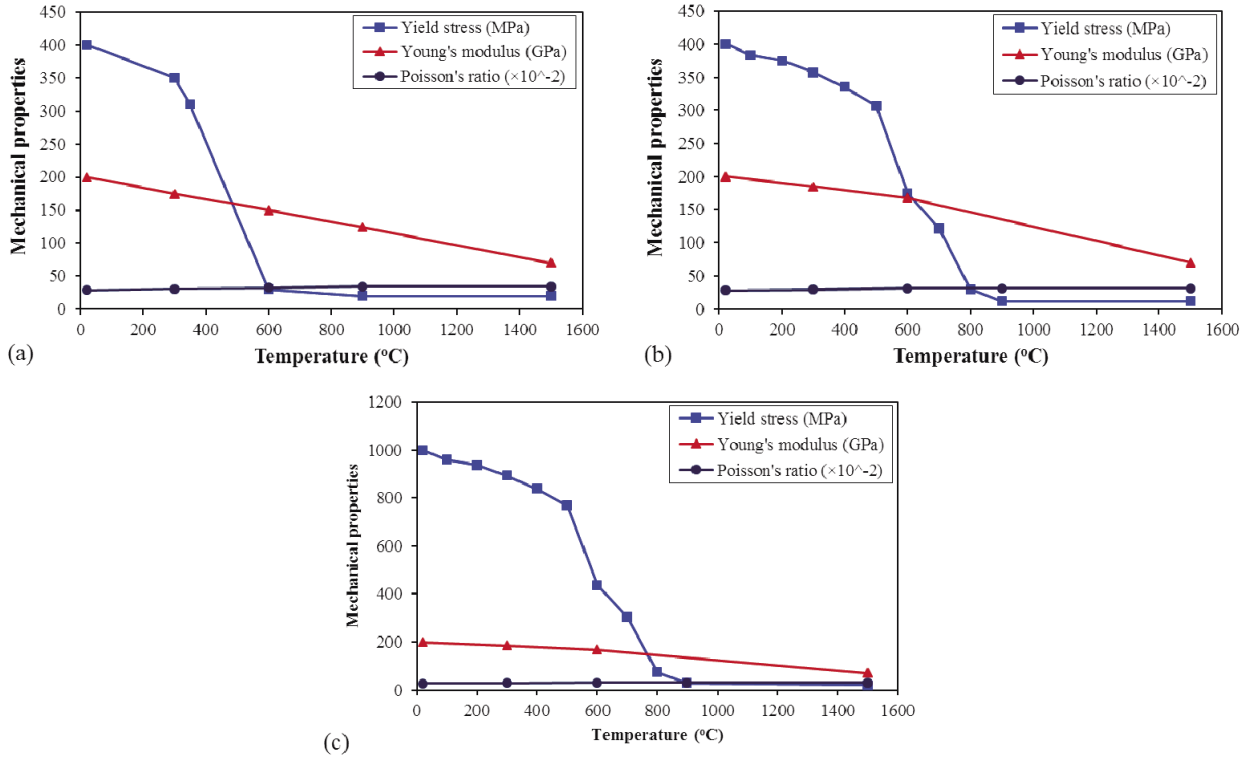

Fig. 4 Temperature-dependent mechanical properties. (a) phase A, (b) phase B and (c) phase C.

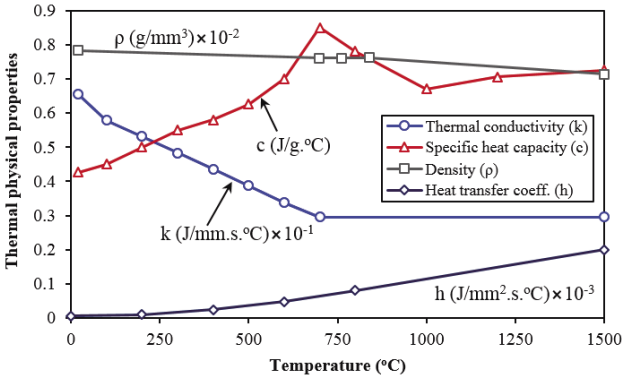

Fig. 5 Temperature-dependent thermal physical properties of butt welded joint models.

properties change during austenitic to ferritic/martensitic transformation. **Figure 6** shows the change of yield strength during austenitic to ferritic phase transformation (i.e. mixture law) for both conventional weld metal and base metal. Similarly, **Fig. 6 (b)** and **(c)** shows how yield strength changes during austenitic to martensitic phase transformation in case of LTT weld wires with different martensitic transformation start temperatures (T_{Ms}). During heating process the yield strength changes with temperature along the solid curve. When the temperature is higher than A_3 (in the weld zone or heat-affected zone), the initial phase (microstructure) which is ferrite in case of both conventional weld wire and base metal and martensite in case of LTT weld wires; will completely transform into austenite. During cooling stage, before the temperature cools down to T_{Fs}/T_{Ms}, the microstructure is under-cooling austenite and its yield strength is relatively low. During austenitic to ferritic/martensitic transformation, the yield strength of the mixtures of austenite and ferrite/martensite is determined by the following equations, respectively:

$$\sigma_{Y\,(A-F)} = f_A.\,\sigma_{YA} + f_F.\,\sigma_{YF} \quad (8)$$

$$\sigma_{Y\,(A-M)} = f_A.\,\sigma_{YA} + f_M.\,\sigma_{YM} \quad (9)$$

where $\sigma_{Y\,(A-F)}$ and $\sigma_{Y\,(A-M)}$ are the yield strengths of the mixtures of austenite and ferrite/martensite, respectively, f_A, f_F and f_M are the phase fractions of austenite, ferrite and martensite, respectively, $f_A + f_F = 1$ and $f_A + f_M = 1$; σ_{YA} , σ_{YF} and σ_{YM} are the yield strengths of austenite, ferrite and martensite, respectively [18].

The broken lines in **Fig. 6** show the variation of yield strength during austenite to ferrite/martensite phase transformations.

4.3 Simulation cases

In the present study, the main objective is to examine the influence of in-plane displacements on the quality of reproduced residual stresses using simulated contour method. A butt welded FE model is selected as a research object for sake of simplicity. As mentioned above, a fine element size that faces the cut surface and a fine mesh density around cutting plane are used in the present FE model. The mesh of FE model and its dimensions are shown in **Fig. 7**. A bead-on-plate weld using GMAW with different weld wires (i.e. conventional and LTT weld wires) is performed in the center and along the model length. The six arrows in **Fig. 7** represent restraint conditions for welding, and these

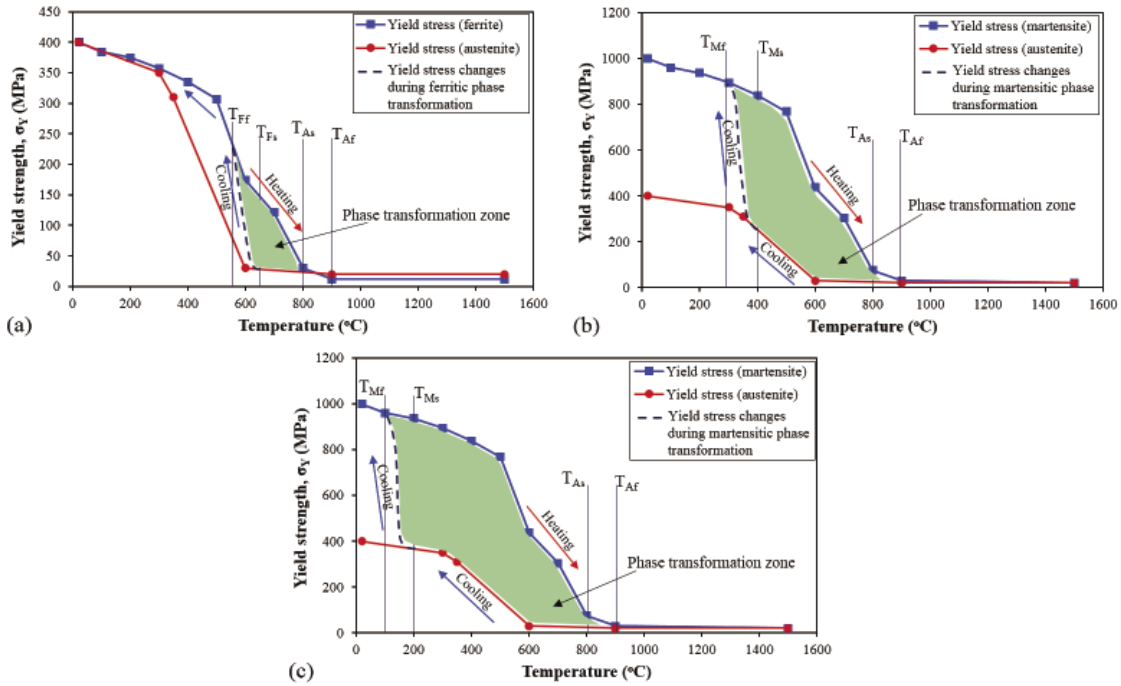

Fig. 6 Temperature-dependent yield strengths of (a) conventional weld wire and base metal, (b) LTT weld wire with T_{Ms} = 400 °C, and (c) LTT weld wire with T_{Ms}= 200 °C. [Note: T_{Fs} and T_{Ff} are ferritic transformation start and finish temperatures, respectively].

conditions are only employed to prevent the rigid body motion. After welding is performed, cutting is carried out at the mid-length of FE model and normal to welding line as shown in **Fig.7**. Thereafter, residual stresses that are originally induced due to welding are reproduced by elastically deforming the cut surface into the opposite shape of the contour using a stress-free model (i.e. using the same FE model as shown in **Fig. 7** but free of stresses). Since the displacements that resulted from stress relaxation have a very small amount compared to the model dimensions, so a non-deformed state (including a flat cut surface) is modeled. On the other hand, in the elastic FE analysis, material behavior is isotropic linearly elastic with Young's modulus of 212 GPa and Poisson's ratio of 0.28.

In this study, three simulation cases are investigated as shown in **Table 2**. In Case A, a conventional weld wire is employed in which both weld and base metals are assumed to have the same properties during cooling process (i.e. ferritic phase transformation as shown in **Fig. 6 (a)**). In Case B, LTT weld wire is used with T_{Ms}= 400 °C. Similarly, in Case C LTT weld wire is employed but with T_{Ms}= 200 °C. Base metal properties for both Case B and Case C are the same as in Case A **(Fig. 6 (a))**. However, weld metal properties for Case B and Case C are assumed to have martensitic phase transformation during cooling process as shown in **Fig. 6 (b)** and **(c)**, respectively. On the other hand to examine the influence of in-plane displacements on the quality of reproduced residual stresses, two computational analyses are performed for each case using 1) both normal and in-plane displacements, and 2) using only normal displacements.

The welding conditions that used in the computational analyses are assumed as follows: welding current = 315 A, arc voltage = 30 V, welding speed = 200 mm/min, and arc efficiency = 85%.

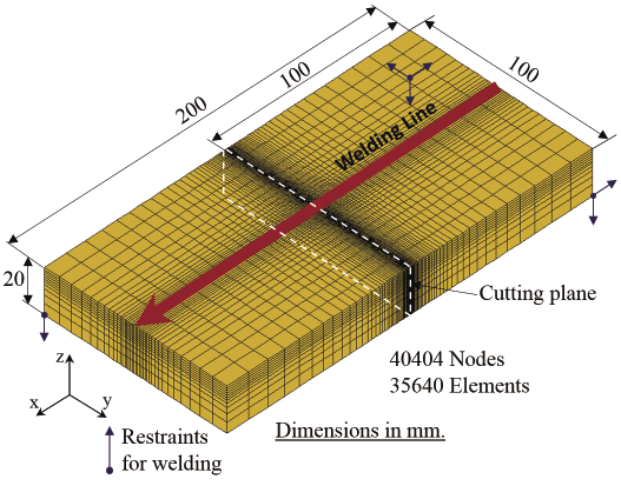

Fig. 7 Finite element model with locations of welding line and cutting plane.

Table 2 Simulation cases with different weld wires.

Case	Wire type	T_{Ms} [°C]
A	Conventional	650
B	LTT	400
C	LTT	200

5. Results and discussion

Figures 8 to **10** show the 2D stress maps of the longitudinal residual stresses predicted by Case A, Case B and Case C, respectively. For the three simulated cases, the 2D stress maps are taken at the cutting plane. **Figure 8** shows a comparison, in which simulated by Case A,

among longitudinal welding residual stresses σ_w, longitudinal reproduced residual stresses using both normal and in-plane displacements σ (*-u*, *-v*, *-w*), and longitudinal reproduced residual stresses σ (*-u*, *free*, *free*) using only normal displacements. It is clear that the 2D stress maps of σ_w and σ (*-u*, *-v*, *-w*) show a very good agreement. However, by comparing the 2D stress map of σ (*-u*, *free*, *free*) with those of σ_w and σ (*-u*, *-v*, *-w*); small differences can be observed. Similar to Case A, **Figs. 9** and **10** show a comparison among σ_w, σ (*-u*, *-v*, *-w*), and σ (*-u*, *free*, *free*) simulated by Case B and Case C, respectively. Comparison between stress maps of σ_w and σ (*-u*, *-v*, *-w*) in both Case B and Case C reveals a very good matching. On the other hand, comparison between stress maps of σ (*-u*, *free*, *free*) and those of σ_w and σ (*-u*, *-v*, *-w*) in both Case B and Case C shows small differences, as shown in **Figs. 9** and **10**. This information tells us that although in-plane displacements have a clear influence on the final longitudinal residual stress distribution; however, the difference in longitudinal residual stresses due to the application of normal displacements only is small for this type of butt welded joint.

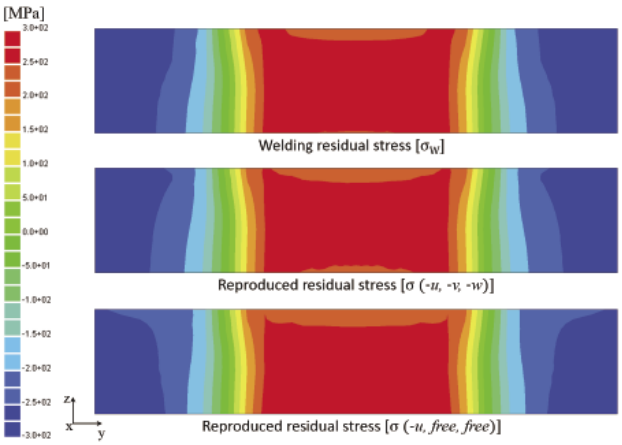

Fig. 8 Longitudinal residual stress 2D maps of Case A.

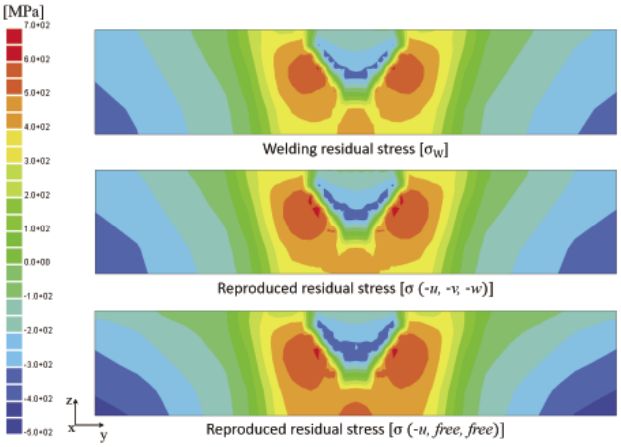

Fig. 9 Longitudinal residual stress 2D maps of Case B.

Through **Figs. 8** to **10** the longitudinal residual stress 2D maps among the three simulation cases were qualitatively compared including σ_w, σ (*-u*, *-v*, *-w*), and σ (*-u*, *free*, *free*). In order to quantitatively compare the simulated results among these cases, the longitudinal residual stress distributions across welding line are plotted at different four locations through thickness at the cut surface; as shown in **Fig. 11**. **Figures 12** to **14** show the longitudinal residual stress distributions at the four locations through thickness across welding line (i.e. at the cutting plane) of the three simulated cases.

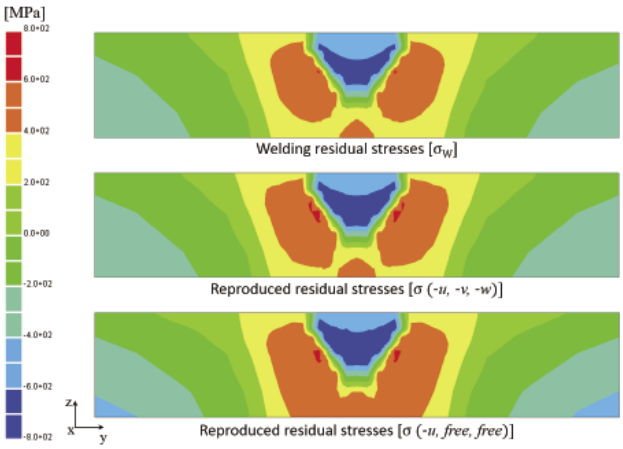

Fig. 10 Longitudinal residual stress 2D maps of Case C.

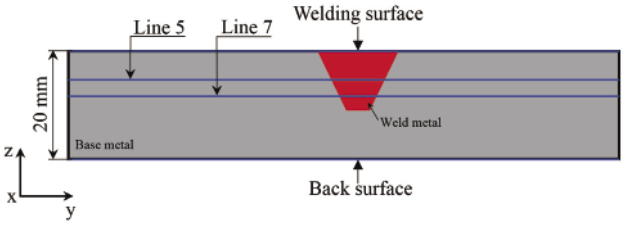

Fig. 11 Schematic drawing of the different locations of longitudinal residual stresses through thickness at the cut surface. [Note: lines 5 and 7 at distances 3 mm and 6 mm from welding surface, respectively].

Figure 12 generally shows a very good agreement among σ_w, σ (*-u*, *-v*, *-w*), and σ (*-u*, *free*, *free*) at the different four locations. On the other hand, carefully comparing σ (*-u*, *free*, *free*) with σ_w and σ (*-u*, *-v*, *-w*), we can find a very slight difference between σ (*-u*, *free*, *free*) and the other two stresses on welding and back surfaces especially beyond the region 15 mm < y < 85 mm. Accordingly, this generally implies that difference between σ (*-u*, *free*, *free*) and the other two stresses is very small and can be neglected for this type of welded joint. Additionally, the influence of in-plane displacements of Case A seems to have minor significant influence on the distribution of longitudinal residual stress in the applied steel.

Moreover, the longitudinal residual stresses in the weld zone (e.g. welding surface, line 5 and line 7) and heat-affected zone (HAZ) of Case A are tensile, in

which these tensile stresses are induced due to the application of conventional weld wire. Further away from the weld zone and HAZ area are the compressive stresses which almost constant near the specimen edges. It is also observed that the tensile stress in the weld center at welding surface, which is the fusion zone of welding, is slightly lower than that away from the center (i.e. HAZ). On the back surface, the residual stresses behave with the same behavior as at welding surface.

Figures 13 and **14** show the longitudinal residual stress distributions simulated by Case B and Case C at the cutting plane. From these figures, comparison among σ_w, σ (*-u*, *-v*, *-w*), and σ (*-u*, *free*, *free*) generally show a good matching. On the other hand when comparing σ (*-u*, *free*, *free*) with the other two stresses on welding surface, a clear difference is noticed **(Figs. 13, 14)** especially in weld zone and beyond the region 20 mm < y < 80 mm. Similarly on the back surface, we can clearly observe the difference between σ (*-u*, *free*, *free*) and the other two stresses **(Figs. 13, 14)**. These differences show the influence of the in-plane displacements on the reproduced residual stresses in the case of applying LTT weld wires. However, these differences have small influence on the quality of reproduced residual stresses for this type of butt welded joint.

The reason why there is a difference between σ (*-u*, *-v*, *-w*) and σ (*-u*, *free*, *free*) especially in case of Case B and Case C is due to when taking the in-plane displacements (*-v*, *-w*) into account; nodes at the cut surface after cutting are forced to return to their original locations as before cutting. This means that each node at the cut surface is forced by the three displacement components (*-u*, *-v*, *-w*) which allow the node to be at its original location. However, when the node at the cut surface is forced only in the normal direction (*-u*) and the in-plane displacements are left to move freely in the reproducing stress step; so this way does not make the node return to its original location exactly as before cutting. Therefore due to the small difference between the nodes locations after forcing them in one direction (*-u*) and their original locations before cutting, the difference between σ (*-u*, *-v*, *-w*) and σ (*-u*, *free*, *free*) is noticed.

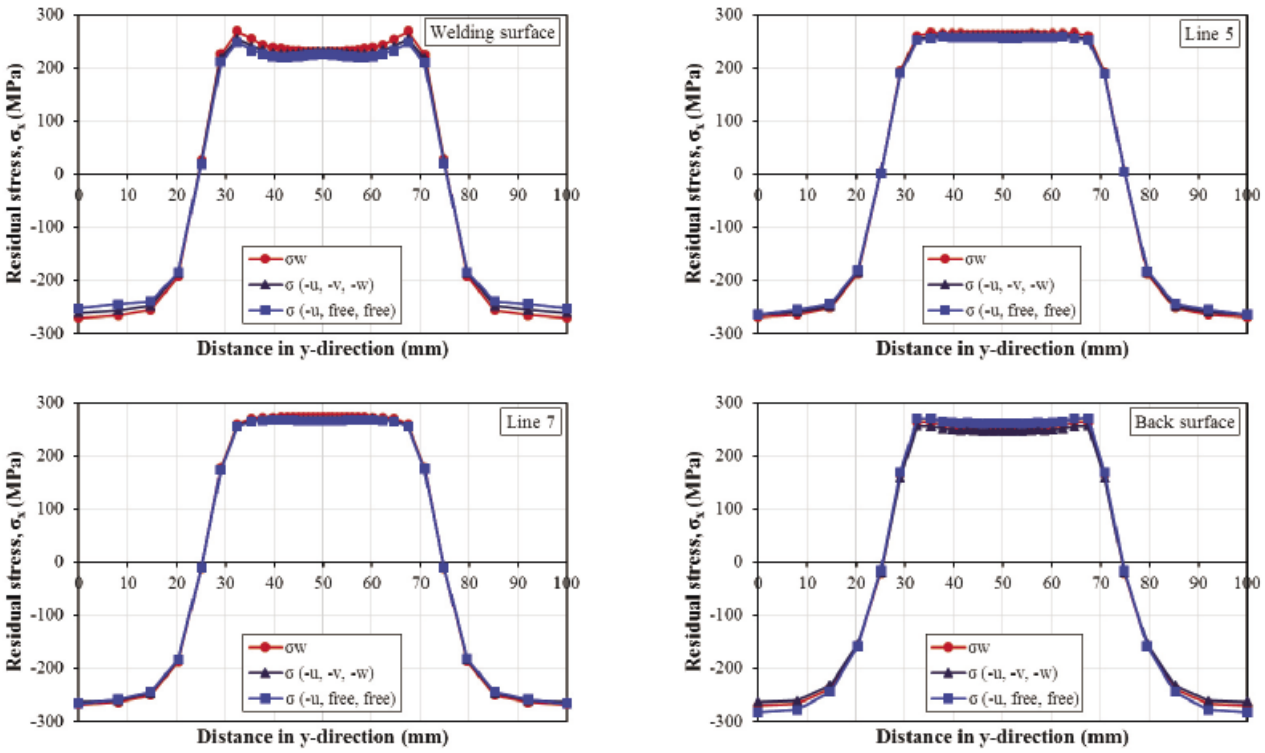

Fig. 12 Longitudinal residual stress distributions of Case A.

On the other hand, **Figs. 13** and **14** show the effectiveness of LTT weld wires in reducing the tensile residual stresses and inducing compressive stresses in the weld zone. To make it more clear, a comparison among longitudinal residual stresses of Case A, Case B and Case C is depicted in **Fig. 15**. Here in **Fig. 15**, we took the reproduced longitudinal residual stress σ (*-u*, *-v*, *-w*) at the welding surface as an example to explain the influence of phase transformation start temperature on the induced longitudinal residual stresses. It is very clear that the longitudinal residual stress simulated by Case A (tensile) is significantly different from those of the other two cases (compressive). This indicates that LTT weld wires (i.e. martensitic transformation start temperatures) largely have influences on the longitudinal residual stress both in magnitude and in distribution. On the other hand, difference between longitudinal residual stress of Case B and that of Case C is notable. This reveals the influence of martensitic transformation start temperature of LTT weld wire on the longitudinal residual stress especially in

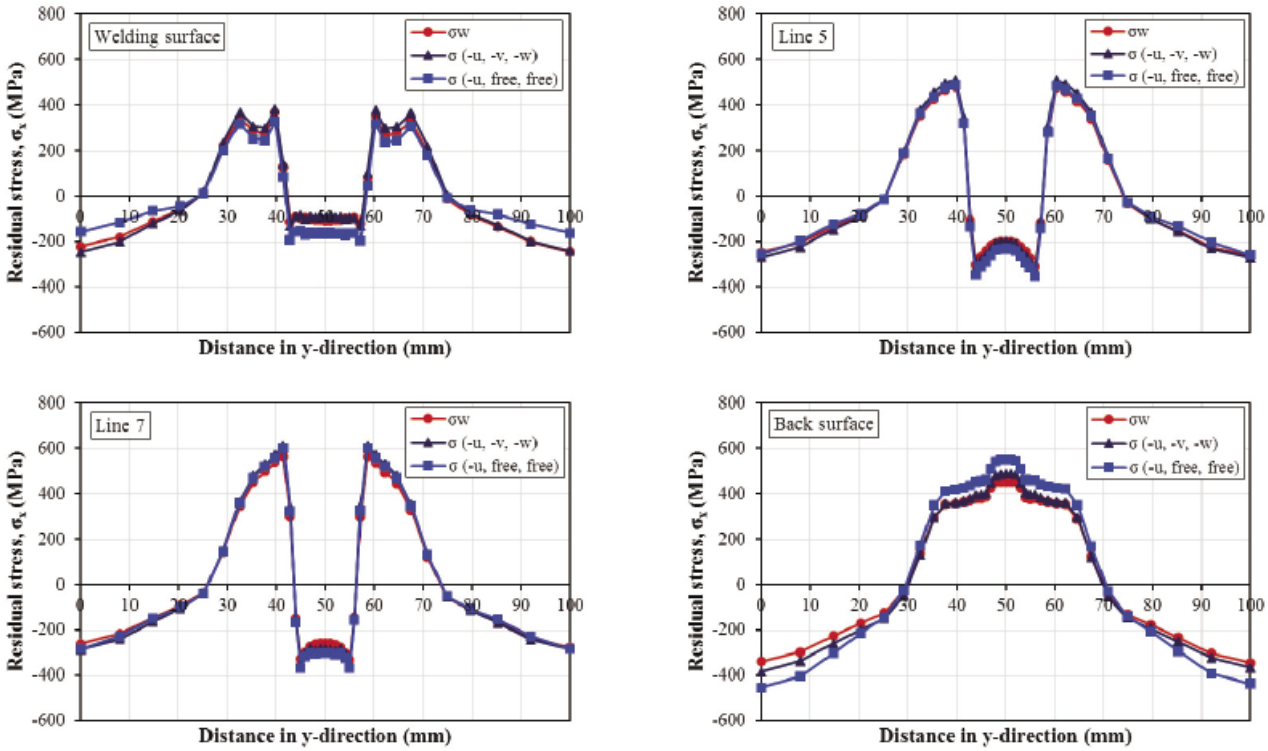

Fig. 13 Longitudinal residual stress distributions of Case B.

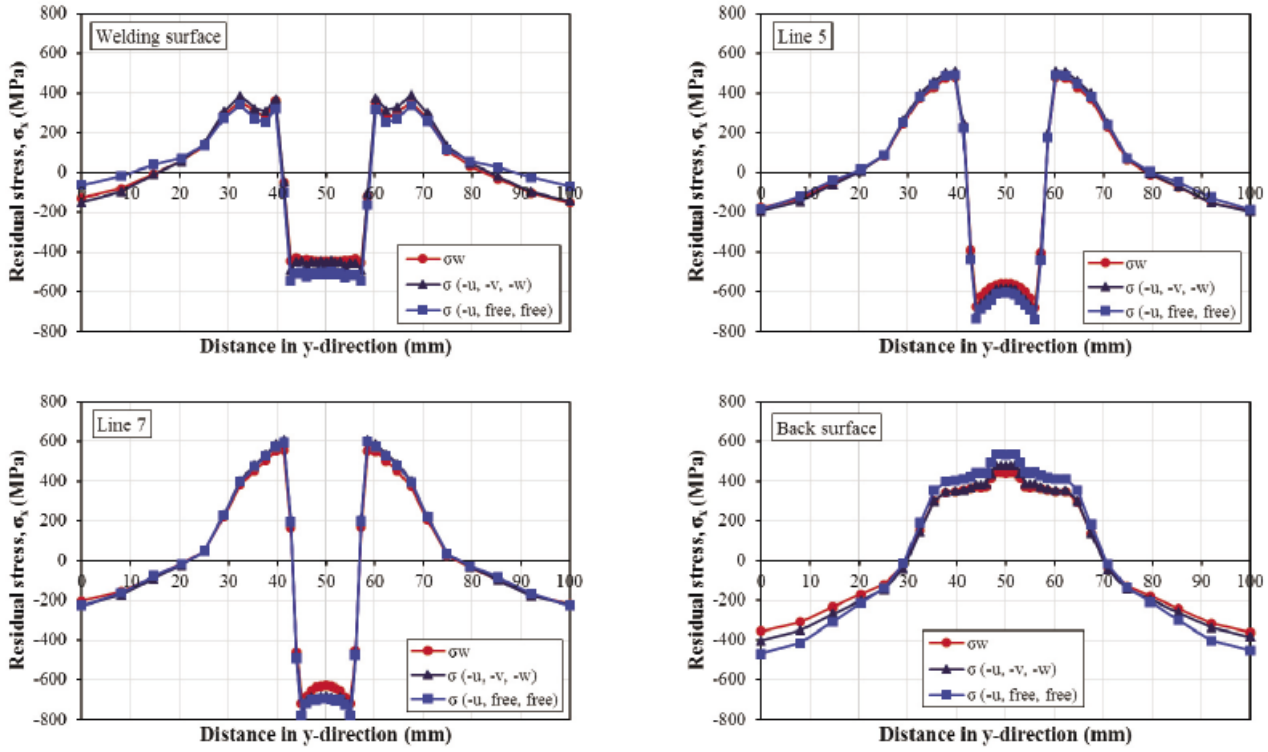

Fig. 14 Longitudinal residual stress distributions of Case C.

weld zone. If we pay attention to the weld zone, it can be observed that the difference of longitudinal residual stress between Case A and Case B at the center of weld is around 325 MPa and that between Case A and Case C at the same position is around 685 MPa. This reveals that the more the transformation start temperature decreases during cooling process, up to a certain value, the larger the compressive stresses can be obtained.

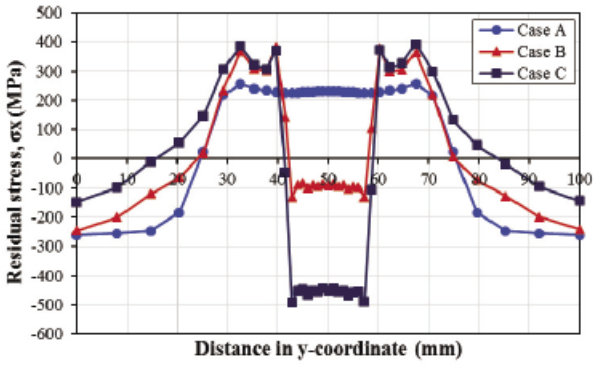

Fig. 15 Comparison of longitudinal residual stresses of the three simulated cases.

6. Conclusions and future work

In this study, a developed computational approach is used to examine the influence of in-plane displacements on the quality of reproduced residual stresses using numerical simulation. In this computational approach, both volume change and mechanical properties variation are considered for LTT weld wires. The developed computational approach is then used to simulate the contour method and reproduce the residual stresses using 1) both normal and in-plane displacements, and 2) using only normal displacements. Based on the simulation results, the following conclusions can be drawn:

(1) A very good agreement between welding residual stresses σ_w and reproduced stresses σ (*-u*, *-v*, *-w*) is achieved for both conventional and LTT welded joint models when the in-plane displacements are considered. This means that in-plane displacements play a significant role in improving the reproduced residual stresses.

(2) Using only normal displacements to the cut surface (*-u*, *free*, *free*) reproduces stresses with a good agreement when compared to σ_w and σ (*-u*, *-v*, *-w*). Accordingly, σ (*-u*, *free*, *free*) can be used in the contour method if sufficient precision of cutting, surface contour measurement and measured data processing is considered.

(3) It is found that as the size of element that faces to the cut surface becomes fine, the error of the computed stress due to FEM data processing decreases and this leads to more precise calculated stresses. So for accurate results of the reproduced residual stresses, fine cutting element size as well as fine mesh density around cutting plane must be used.

(4) Simulated contour method successfully provides 2D stress maps for welding and reproduced residual stresses which reveal the behavior of calculated residual stresses in weld metal for conventional and LTT welded joints. Tensile residual stresses are introduced in the weld in the case of applying conventional weld wire, however; compressive stresses resulted in the weld by applying LTT wires.

(5) In this research, the influence of both normal and in-plane displacements besides using only normal displacements on the quality of reproduced residual stresses using numerical simulation is examined. Accordingly, it is necessary to perform experiment to include welding using different weld wires and applying the contour method to measure the produced residual stresses to verify the developed computational approach by comparing the simulated results with the measured one.

Acknowledgments

Authors gratefully thank Prof. Sherif Rashed for the fruitful discussions and comments.

References

[1] T. Kannengiesser, A. Kromm, M. Rethmeier, J. Gibmeier, and C. Genzel “Residual stresses and in-situ measurement of phase transformation in low transformation temperature (LTT) welding materials”, JCPDS - Int. Cent. Diffr. Data, pp. 755–762, 2009.

[2] J. Altenkirch, J. Gibmeier, A. Kromm, T. Kannengiesser, T. Nitschke-Pagel, and M. Hofmann “In situ study of structural integrity of low transformation temperature (LTT)-welds”, Mater. Sci. Eng. A, vol. 528, no. 16–17, pp. 5566–5575, 2011.

[3] Z. Barsoum and M. Gustafsson “Fatigue of high strength steel joints welded with low temperature transformation consumables”, *Eng. Fail. Anal.*, vol. 16, no. 7, pp. 2186–2194, 2009.

[4] C. Miki and K. Anami “Improving Fatigue strength by addtional welding with low temperature transformation welding electrodes”, *Steel Struct.*, vol. 1, pp. 25–32, 2001.

[5] A. Ota, Y. Maeda, N. Suzuki, O. Watanabe, T. Kubo, and K. Katsuoka “Fatigue strength improvement of box welds using low transformation temperature welding material . Tripled fatigue strength by post weld heat treatment”, *Weld. Int.*, vol. 16, no. 1, pp. 44–47, 2002.

[6] A. A. Bhatti, Z. Barsoum, V. V. D. Mee, A. Kromm, and T. Kannengiesser “Fatigue strength improvement of welded structures using new low transformation temperature filler materials”, *Procedia Eng.*, vol. 66, pp. 192–201, 2013.

[7] P. P. Darcis, H. Katsumoto, M. C. Payares-Asprino, S. Liu, and T. A. Siewert “Cruciform fillet welded joint fatigue strength improvements by weld metal phase transformations”, *Fatigue Fract. Eng. Mater. Struct.*, vol. 31, no. 2, pp. 125–136, 2008.

[8] S. H. Thomas and S. Liu “Analysis of low transformation temperature welding (LTTW) consumables – Distortion control and evolution of stresses”, *Sci. Technol. Weld. Join.*, vol. 19, no. 5, pp. 392–401, 2014.

[9] N. S. Rossini, M. Dassisti, K. Y. Benyounis, and A. G. Olabi “Methods of measuring residual stresses in components”, *Mater. Des.*, vol. 35, pp. 572–588, 2012.

[10] P. Pagliaro, M. B. Prime, H. Swenson, and B. Zuccarello “Measuring multiple residual-stress components using the contour method and multiple cuts”, *Exp. Mech.*, vol. 50, no. 2, pp. 187–194, 2010.
[11] M. B. Prime and A. L. Kastengren “The contour method cutting assumption : Error minimization and correction”, *Exp. Appl. Mech.*, vol. 6, pp. 233–250, 2011.
[12] M. B. Prime, M. R. Hill, A. T. Dewald, R. J. Sebring, V. R. Dave, and M. J. Cola “Residual stress mapping in welds using the contour method”, in *Trends in Welding Research, Proceedings of the 6th International Conference*, 2003, vol. 836, pp. 891–896.
[13] M. Turski and L. Edwards “Residual stress measurement of a 316L stainless steel bead-on-plate specimen utilising the contour method”, *Int. J. Press. Vessel. Pip.*, vol. 86, no. 1, pp. 126–131, 2009.
[14] Y. Zhang, S. Ganguly, L. Edwards, and M. E. Fitzpatrick “Cross-sectional mapping of residual stresses in a VPPA weld using the contour method”, *Acta Mater.*, vol. 52, no. 17, pp. 5225–5232, 2004.
[15] C. Liu and X. Yi “Residual stress measurement on AA6061-T6 aluminum alloy friction stir butt welds using contour method”, *Mater. Des.*, vol. 46, pp. 366–371, 2013.
[16] L. Hacini, N. Van Lê, and P. Bocher “evaluation of residual stresses induced by robotized hammer peening by the contour method”, *Exp. Mech.*, vol. 49, pp. 775–783, 2009.
[17] N. Murugan and R. Narayanan “Finite element simulation of residual stresses and their measurement by contour method”, *Mater. Des.*, vol. 30, no. 6, pp. 2067–2071, 2009.
[18] D. Deng and H. Murakawa “Influence of transformation induced plasticity on simulated results of welding residual stress in low temperature transformation steel”, *Comput. Mater. Sci.*, vol. 78, pp. 55–62, 2013.